Propagation of short intense laser pulses in gas-filled capillaries

N. E. Andreev*
Institute for High Energy Densities, Associated Institute for High Temperatures, Russian Academy of Sciences, Izhorskaya 13/19, Moscow 127412, Russia

Y. Nishida and N. Yugami
Department of Energy and Environmental Science, Graduate School of Engineering, Utsunomiya University, 7-1-2 Yoto, Utsunomiya, Tochigi 321-8585, Japan

(Received 22 October 2001; published 2 May 2002)

The guided laser pulse propagation and wake-field generation are studied in a wide (in comparison with the laser spot size) gas-filled capillary with an on-axis gas density depletion, which can be produced by a rapid spin of the capillary around its axis or by radially propagating shock waves generated in a piezoceramic tube. A single equation for the wake-field potential, which describes the fully relativistic plasma response in the presence of optical field ionization (OFI) of a gas, is derived and used to demonstrate a guided propagation of a short intense laser pulse over many Rayleigh lengths in a leaky plasma channel produced by the pulse due to OFI in the capillary filled with a radially inhomogeneous gas. The efficient generation of a regular wake field over long distances suitable for the laser wake-field accelerators is shown.

DOI: 10.1103/PhysRevE.65.056407 PACS number(s): 52.50.Jm, 42.65.Tg, 41.20.Jb, 41.75.Jv

I. INTRODUCTION

Optical guiding of short intense laser pulses over many Rayleigh lengths is important in many applications such as laser-driven plasma accelerators [1], harmonic generation [2,3], and x-ray lasers [4,5]. There are several mechanisms and methods to increase the length of intense laser pulse propagation in plasmas. One of them is relativistic focusing and ponderomotive channeling [6,7]. Preformed plasma channels provide another possibility for long distance guiding of laser pulses [8–10]. Such channels with an on-axis minimum of the plasma density have been realized by axicon-focused lasers [11–13], by slow electrical discharges in initially evacuated capillaries [14,15], by a *Z*-pinch discharge in gas-filled capillaries [16], or by a slow discharge through a hydrogen-filled capillary when the pinch effect is negligible [17].

An alternative approach is based on the use of capillary tubes as a guiding structure when the laser pulse is guided by the tube's inner wall, while the plasma can be created by optical field ionization of a gas filling the capillary [18]. Multimode guiding of terawatt laser pulses through comparatively wide (with diameters of order 100 μm) hollow capillary tubes was demonstrated first in [19,20]. This multimode regime is characterized by a complex transverse intensity profile and leads to inner wall breakdown at high laser intensities [19]. Monomode guiding of intense laser pulses (10^{16} W/cm^2) over 100 Rayleigh lengths in capillary dielectric tubes was investigated experimentally in [21]. Experiments with higher pulse intensities guided in a monomode regime, characterized by lower energy losses through the walls, are now in progress with dielectric hollow tubes and gas-filled capillaries [18].

In the present paper we investigate a new possibility of channel-guided propagation of short intense laser pulses and wake-field generation in wide (in comparison with the laser spot size) gas-filled capillaries. A radial profile of a gas with minimum on-axis density considered below can be obtained by the rapid spin of a capillary around its axis, or by using piezoceramic tubes [22]. To provide the rapid spin of a tiny capillary a rotating magnetic field can be used if the capillary wall is double layered, the internal part of which could be a dielectric material or metal and the outside thin layer could be a magnetic one made by sputtering or deposition. This technique is available now, but not realized yet, so the precise characteristics of the system should be discussed and tested experimentally later on.

An intense laser pulse propagating in a capillary filled with this inhomogeneous gas density will produce by optical field ionization a leaky plasma channel, in which the plasma density has an on-axis minimum and also decays to zero at the capillary walls, where the laser pulse intensity is too low to ionize a gas. This channel may provide the desired guiding effect to propagate tightly focused laser pulses over distances of many Rayleigh lengths.

The paper is organized as follows. The equations for the laser envelope that take finite pulse length effects into account, and also for the wake-field generation, are derived in Sec. II. The set of basic equations was formulated with allowance made for the following processes: tunneling gas ionization [23], the nonlinear contribution from the bound atomic electrons to the dielectric constant of a gas inside a capillary [24], the fully relativistic plasma response of free electrons governing the relativistic and ponderomotive self-focusing of a powerful laser pulse and the wake-field generation, and the laser energy losses in the process of optical field ionization (OFI) [25,26]. The model boundary conditions at the capillary wall were used for a one-component linear polarized laser pulse. The results of numerical simulations of a guided propagation of short intense laser pulses in

*Electronic address: andreev@laslab.ras.ru

wide gas-filled capillaries are presented in Sec. III, and a conclusion is given in Sec. IV.

II. BASIC EQUATIONS

A. Laser pulse propagation

The laser pulse propagation in a gas-filled capillary can be described by the following Maxwell's wave equation for the envelope of the pulse (compare [24]):

$$\left\{ 2ik_0\left(\frac{\partial}{\partial z}+c^{-1}\varepsilon_0\frac{\partial}{\partial t}\right)+\Delta_\perp+k_0^2(\varepsilon_0-1)+\frac{\partial^2}{\partial z^2} -c^{-2}\varepsilon_0\frac{\partial^2}{\partial t^2}\right\}\boldsymbol{E}_0=k_0^2\left(\frac{n}{n_c\gamma}-\delta\varepsilon_a^{(NL)}\right)\boldsymbol{E}_0-4\pi i\frac{\omega_0}{c^2}\boldsymbol{J}^{(ion)}, \tag{1}$$

where the slowly varying (on the time and spatial scales ω_0^{-1} and $k_0^{-1}=c/\omega_0$, which are the inverse frequency and wave number of laser radiation) complex amplitude of the laser field $\boldsymbol{E}_0$ is related to the (high frequency) electric field of the laser pulse $\tilde{\boldsymbol{E}}$ by the expression

$$\tilde{\boldsymbol{E}}=\mathrm{Re}\{\boldsymbol{E}_0\exp[-i\omega_0 t+ik_0 z]\}. \tag{2}$$

In Eq. (1) $\Delta_\perp$ is a transverse part of the Laplace operator, ε_0 is a linear dielectric constant of the bound electrons of a gas (inside a capillary, $r_\perp<R_{cap}$, $\varepsilon_0\cong 1$), or dielectric walls at $r_\perp\geqslant R_{cap}$, where $\varepsilon_0=\varepsilon_w>1$; $\delta\varepsilon_a^{(NL)}=2\eta_2 I_L$ is the nonlinear contribution from the bound atomic electrons to the dielectric constant of a gas inside a capillary ($\eta_2 I_L=\Delta\eta_a$ is the corresponding contribution to the refractive index, $I_L=(c/8\pi)|\boldsymbol{E}_0|^2$ is the time averaged laser intensity). The density of free (plasma) electrons is n and $n_c=m\omega_0^2/(4\pi e^2)$ is the critical density for the laser frequency ω_0, γ is the relativistic factor of plasma electrons and will be specified in the following section. The ionization current $\boldsymbol{J}^{(ion)}$ describes the laser energy losses in the process of OFI [25,26] and consists of two parts: one is proportional to the ionization energy (potentials of ionization of atoms and ions) [27,28], and second one originates from the second harmonic of electron production rate (see below) and describes the part of residual energy [29] irreversibly transferred to electrons due to nonadiabatic laser-electron interaction during OFI [30]. It should be noted that in the capillary walls at $r_\perp\geqslant R_{cap}$ the right-hand side of Eq. (1) equals zero, and also the dielectric constant $\varepsilon_0=\varepsilon_w$ should be omitted in the terms proportional to the time derivatives in the left-hand side of Eq. (10) for a metal wave guide.

Inside a capillary we can neglect a small difference ε_0-1 (due to a small linear polarization of a gas) and using the dimensionless comoving with the laser pulse variables

$$\xi=k_{p0}(z-ct),\quad \zeta=k_{p0}z,\quad \boldsymbol{\rho}=k_{p0}\boldsymbol{r}_\perp, \tag{3}$$

we can rewrite Eq. (1) in the form

$$\left\{2i\frac{\partial}{\partial\zeta}+\frac{k_{p0}}{k_0}\left(\Delta_{\perp\rho}+2\frac{\partial^2}{\partial\zeta\partial\xi}\right)\right\}\boldsymbol{a} =\frac{k_{p0}}{k_0}\left[\left(\frac{\nu}{\gamma}-\frac{3}{8}R|\boldsymbol{a}|^2\right)\boldsymbol{a}-i\boldsymbol{G}^{(ion)}\right], \tag{4}$$

where $\boldsymbol{a}=e\boldsymbol{E}_0/(mc\omega_0)$ is a dimensionless laser envelope, $\nu=n/\mathcal{N}_0$ is the normalized (by a given constant $\mathcal{N}_0$) electron density, $k_{p0}=\omega_{p0}/c=(4\pi e^2\mathcal{N}_0/m)^{1/2}/c$ is a normalizing inverse space scale (which can be equal, e.g., to the maximum value of the plasma wave number at the capillary axis, if $\mathcal{N}_0$ is chosen as a maximum value of the electron plasma density produced by OFI at the axis), and $R=P_c/P_a$ is the ratio of critical powers for the relativistic self-focusing in a plasma [$P_c\cong 17(\omega_0/\omega_p)^2$ GW] and for the nonlinear focusing in a gas [$P_a\cong 2\pi(k_0^2\eta_2)^{-1}$] [24]. The ionization losses described by $\boldsymbol{G}^{(ion)}=(4\pi e/m\omega_{p0}^2 c)\boldsymbol{J}^{(ion)}$ will be explicitly defined in the following section.

B. Nonlinear plasma response

To describe the slowly varying (on the time scale ω_0^{-1}) motions and fields in a plasma we use Maxwell's equations and the relativistic hydrodynamic equations for cold plasma electrons [31] with allowance made for the process of tunneling gas ionization included in the base of the kinetic description [32,25]:

$$\frac{\partial\boldsymbol{p}}{\partial t}=e\boldsymbol{E}-mc^2\nabla\gamma-\frac{\Gamma_0}{n}\boldsymbol{p}+\frac{1}{2}\frac{mc}{n} \times\left(\Gamma_0|\boldsymbol{a}|^2-\frac{1}{2}\mathrm{Re}\{\Gamma_2(\boldsymbol{a}^*\cdot\boldsymbol{a}^*)\}\right)\boldsymbol{e}_z, \tag{5}$$

$$\frac{\partial n}{\partial t}+\mathrm{div}(n\boldsymbol{v})=\Gamma_0\equiv\frac{\partial n_0}{\partial t}, \tag{6}$$

$$\frac{\partial\boldsymbol{E}}{\partial t}=-4\pi en\boldsymbol{v}+c\,\mathrm{rot}\,\boldsymbol{B}, \tag{7}$$

$$\mathrm{rot}\,\boldsymbol{E}=-\frac{1}{c}\frac{\partial\boldsymbol{B}}{\partial t}, \tag{8}$$

where $\boldsymbol{p}$ is the electron momentum connected with the velocity of electrons by the relation $\boldsymbol{v}=\boldsymbol{p}/(m\gamma)$, n is the density of the plasma electrons, n_0 is zero harmonic of the electron density produced by OFI, Γ_0 and Γ_2 are zero and second harmonics of the electron production rate, $\boldsymbol{E}$ and $\boldsymbol{B}$ are the slowly varying electric and magnetic fields, and γ is the relativistic factor of electrons,

$$\gamma=\left[1+\left(\frac{\boldsymbol{p}}{mc}\right)^2+\frac{1}{2}|\boldsymbol{a}|^2\right]^{1/2}. \tag{9}$$

The dynamics of plasma formation due to tunneling ionization of a gas in the field of a short intense laser pulse is described by the equations of ionization kinetics for the densities N_k of ions with ionization multiplicity k (k

$=0,1\ldots,Z_n-1$, where Z_n is the charge number of an atom nucleus). The electron production rate (N_e is the electron density produced by OFI)

$$\Gamma=\frac{\partial N_e}{\partial t}\equiv\sum_{k=1}^{Z_n} k\frac{\partial N_k}{\partial t}=\sum_{k=0}^{Z_n-1} W_k N_k\equiv\sum_{k=0}^{Z_n-1}\Gamma^{(k)} \quad (10)$$

is governed by the probabilities W_k of tunneling ionization per unit time for ions with multiplicity k, which are determined by the well-known Ammosov-Delone-Krainov (ADK) formula [23]. In the processes of tunneling ionization, Γ oscillates in time (if the laser pulse is not circularly polarized) and includes the zeroth and higher even harmonics of the laser pulse frequency,

$$\Gamma=\Gamma_0+\mathrm{Re}\left\{\sum_{n=1}^{\infty}\Gamma_{2n}\exp(-2in\omega_0 t)\right\}. \quad (11)$$

These should be taken into account in studies of the laser pulse propagation in an ionizing gas and wake-field generation in a plasma produced by the laser pulse [25–30,33]. As a consequence we allow for zeroth (Γ_0) and the second (Γ_2) harmonics of the electron source Γ, Eq. (10). For a wide range of gases and laser pulse parameters $\Gamma_2\approx 2\mu\Gamma_0$, where $\mu=0.7$–1 [25,26]. The zeroth harmonic of the electron source Γ_0 should be calculated using the envelope amplitude of the laser pulse in the averaged over a laser period ADK formula for $\overline{W}_k(|\boldsymbol{E}_0|)$ [23,29]. The equations of ionization kinetics for ion densities $\overline{N}_k$ averaged over a laser period can be written in the form

$$\frac{\partial D_0}{\partial t}=-\overline{W}_0 D_0,$$
$$\frac{\partial D_k}{\partial t}=[\overline{W}_{k-1}D_{k-1}-\overline{W}_k D_k],\quad k=1,2,\ldots Z_n-1, \quad (12)$$

where $D_k=\overline{N}_k/n_a$ are the relative ion densities normalized to the time independent (but can be inhomogeneous) gas density, which in turn equals the total ion density (including neutrals) $n_a(\boldsymbol{r})=\Sigma_{k=0}^{Z_n}N_k$. The solution to Eqs. (12) makes it possible to define the zeroth harmonic of the electron density produced by OFI ($n_0=\overline{N}_e$) and the electron production rate $\Gamma_0=\overline{\Gamma}$,

$$n_0=n_a\left\{(1-D_0)Z_n-\sum_{k=1}^{Z_n-1}(Z_n+1-k)D_k\right\},$$
$$\Gamma_0=n_a\sum_{k=0}^{Z_n-1}\overline{W}_k D_k\equiv\sum_{k=0}^{Z_n-1}\Gamma_0^{(k)}. \quad (13)$$

In the quasistatic approximation [34], by using the dimensionless comoving variables (3), the set of Eqs. (5)–(8) can be written in the form

$$\frac{\partial}{\partial\xi}(\boldsymbol{e}_z\gamma-\boldsymbol{q})=\boldsymbol{E}-\boldsymbol{\nabla}_\perp\gamma-\frac{S_0}{\nu}\left(\boldsymbol{q}-\frac{1}{2}|\boldsymbol{a}|^2\boldsymbol{e}_z\right)$$
$$-\frac{1}{8\nu}\mathrm{Re}\{S_2(\boldsymbol{a}^*\cdot\boldsymbol{a}^*)\}\boldsymbol{e}_z, \quad (14)$$

$$\frac{\partial}{\partial\xi}[(u_z-1)\nu]+\partial_\perp(\nu\boldsymbol{u}_\perp)=S_0\equiv-\frac{\partial\nu_0}{\partial\xi}, \quad (15)$$

$$\left[\frac{\partial^2\boldsymbol{E}}{\partial\xi^2}+\boldsymbol{\nabla}\times\boldsymbol{\nabla}\times\boldsymbol{E}\right]=\frac{\partial}{\partial\xi}(\nu\boldsymbol{u}), \quad (16)$$

where $\Delta_\perp$ and $\partial_\perp$ are transverse parts of the gradient and divergence; $\nu=n/\mathcal{N}_0$ is the total (slowly varying) normalized electron density [the same as in Eq. (4)], which describes the nonlinear plasma response to the ponderomotive action of the laser pulse, namely, the wake-field generation, with consideration for the tunneling ionization processes; $\nu_0=n_0/\mathcal{N}_0$ is the normalized zero harmonic of electron density produced by the optical field ionization; $\boldsymbol{q}=\boldsymbol{p}/mc$, $\boldsymbol{u}=\boldsymbol{v}/c$, and $\boldsymbol{E}=e\boldsymbol{E}/(mc\omega_{p0})$ are the dimensionless electron momentum, velocity, and slowly varying electric field consequently. The normalized zero and second harmonics of the electron production rate (11) are determined by the solution to Eqs. (12) as follows:

$$S_0=\frac{\Gamma_0}{\mathcal{N}_0\omega_{p0}}=\frac{n_a}{\mathcal{N}_0\omega_{p0}}\sum_{k=0}^{Z_n-1}\overline{W}_k D_k\equiv\sum_{k=0}^{Z_n-1}S_0^{(k)},$$
$$S_2=\frac{\Gamma_2}{\mathcal{N}_0\omega_{p0}}\cong 2\mu S_0. \quad (17)$$

The normalized ionization current in Eq. (4) can be explicitly expressed through the harmonics of the ionization source (17),

$$\boldsymbol{G}^{(ion)}=\frac{4\pi e}{m\omega_{p0}^2 c}\boldsymbol{J}^{(ion)}=\frac{k_{p0}}{k_0}\left[\frac{2\boldsymbol{a}}{|\boldsymbol{a}|^2}\sum_{k=0}^{Z_n-1}S_0^{(k)}\frac{U_k}{mc^2}-\frac{\boldsymbol{a}^*S_2}{4}\right], \quad (18)$$

where U_k is the ionization potential of ions with multiplicity k to ionization multiplicity $k+1$.

The nonlinear relativistic plasma response ν/γ [for background density ν_0 known from Eqs. (12) and (13) produced by OFI] can be expressed in accordance with Eqs. (14)–(16) through a single scalar function (potential) Φ (compare [35]),

$$\frac{\nu}{\gamma}=\frac{\nu_0+\Delta_\perp\Phi}{\Phi+\delta\Phi_S}, \quad (19)$$

where the potential, taking into consideration the birth of free electrons due to the gas ionization, is defined as follows [with the boundary condition $\Phi(\xi\to+\infty)=1$]:

$$\Phi=\gamma-q_z+\int_{+\infty}^{\xi}\frac{S_0}{\nu}\left(q_z-\frac{|\boldsymbol{a}|^2}{2}-\frac{\mu}{4}\mathrm{Re}(\boldsymbol{a}^*\cdot\boldsymbol{a}^*)\right)d\xi' \equiv\gamma-q_z-\delta\Phi_S, \tag{20}$$

and the last integral term in this expression can be written through the same potential Φ,

$$\delta\Phi_S=-\frac{1}{\nu_0}\int_{+\infty}^{\xi}\frac{\partial\nu_0}{\partial\xi'}\left(\Phi-1+\frac{|\boldsymbol{a}|^2}{4}-\frac{\mu}{4}\mathrm{Re}(\boldsymbol{a}^*\cdot\boldsymbol{a}^*)\right)d\xi'. \tag{21}$$

The dimensionless components of electric and magnetic fields in plasma, and so the forces acting on an accelerated relativistic electron, can also be expressed through the potential Φ,

$$F_z=E_z=\frac{\partial\Phi}{\partial\xi},\quad F_r=E_r-B_\varphi=\frac{\partial\Phi}{\partial\rho}, \tag{22}$$

where in the last expression the axial symmetry of the problem is assumed.

The equation for the potential can be obtained from Eqs. (14)–(16) taking into account Eqs. (19) and (22),

$$\frac{\partial^2\Phi}{\partial\xi^2}+\partial_\rho E_r=\frac{\nu_0+\Delta_\perp\Phi}{\Phi+\delta\Phi_S}\gamma-\nu_0, \tag{23}$$

where

$$\partial_\rho=\frac{1}{\rho}\frac{\partial}{\partial\rho}\rho\quad\text{and}\quad\Delta_\perp=\frac{1}{\rho}\frac{\partial}{\partial\rho}\rho\frac{\partial}{\partial\rho}$$

are transverse parts of the divergence and Laplace operator,

$$E_r=\frac{\partial\gamma}{\partial\rho}-\frac{\Phi+\delta\Phi_S}{\nu_0+\Delta_\perp\Phi}\frac{\partial^3\Phi}{\partial\rho\partial\xi^2}-q_r\left[\frac{1}{\gamma}\frac{\partial\gamma}{\partial\xi}-\frac{\partial(\nu-\nu_0)}{\nu\partial\xi}\right], \tag{24}$$

$$q_r=\frac{\Phi+\delta\Phi_S}{\nu_0+\Delta_\perp\Phi}\frac{\partial^2\Phi}{\partial\rho\partial\xi}, \tag{25}$$

$$\gamma=\frac{1}{2}\left[\frac{1+q_r^2+|\boldsymbol{a}|^2/2}{\Phi+\delta\Phi_S}+\Phi+\delta\Phi_S\right]. \tag{26}$$

Equations (19), (21), and (24)–(26) show that in the presence of ionization (of comparatively light gases) the description of the strongly nonlinear plasma response to the action of an ultrahigh intense laser pulse can be exactly reduced to a single equation (23) for the potential (20), similarly to the case of preionized plasma [36]. But in the presence of optical field ionization this equation should be evidently supplemented with the ionization kinetics (12), (13), which describes the creation of the ''background'' density of free plasma electrons n_0. Note that even in an homogeneous gas, the background electron density produced by OFI is very inhomogeneous in both radial and longitudinal (local time ξ) directions that make the self-consistent solution of Eqs. (4) and (23) much more complicate then in preformed plasma.

Nevertheless the simplification of Eqs. (23)–(26) is possible for a wide (in comparison with the plasma skin depth $1/k_p$) laser pulse, having in mind that (for comparatively light gases under consideration) OFI takes place in the regions where the intensity of the laser pulse is much smaller than the relativistic one ($|\boldsymbol{a}|\ll1$) and so, Eq. (23) can be linearized with respect to the small parameter $|\Phi-1|/(k_pL_\perp)^2$. The characteristic scale length in the radial direction $L_\perp$ is high (in comparison with the plasma wavelength for a wide laser pulse) in the regions of high laser intensity (where $|\Phi-1|$ is not small), while $|\Phi-1|\ll1$ in the regions of sharp gradients of the background density n_0, where $L_\perp$ can be of order k_p. In doing so we arrive at the following equation for the potential:

$$\left\{(\Delta_\perp-\nu_0)\frac{\partial^2}{\partial\xi^2}-\frac{\partial\ln\nu_0}{\partial\rho}\frac{\partial^3}{\partial\rho\partial\xi^2}+\nu_0\Delta_\perp\right\}\Phi-\frac{\nu_0^2}{2}\left[1-\frac{1+|\boldsymbol{a}|^2/2}{(\Phi+\delta\Phi_S)^2}\right]=\frac{\nu_0}{4}\Delta_\perp|\boldsymbol{a}|^2. \tag{27}$$

This equation has two exact limits: (a) linear, when $|\boldsymbol{a}|^2<1$, $|\Phi-1|<1$ and Eq. (27) can be transformed into Eq. (7) of Ref. [33]; (b) fully relativistic one-dimensional limit with allowance made for OFI, when $|\Phi-1|/(k_pL_\perp)^2\ll1$ and all transverse derivatives can be neglected.

It should be pointed out that Eq. (27) describes correctly a fully relativistic plasma response to the action of an intense laser pulse without restriction $|a_{max}|^2<1$ if (i) the laser ionizes a gas at low intensities (in the regions where $|a|^2\ll1$), which restricts our consideration to comparatively light gases with low charge numbers of atom nuclei, and (ii) the laser spot size (the characteristic radial scale length of the main, more intensive part of the laser pulse) is in excess of the plasma skin depth $1/k_p$. Further, we shall assume that both these restrictions are fulfilled and shall use Eq. (27) to analyze the intense laser pulse channeling in wide capillaries filled with hydrogen and helium.

C. Boundary conditions at capillary walls

To get the accurate nonstationary boundary conditions at capillary walls we start from the simplified geometry of the problem. Let us consider an *S*-polarized (along the *OX* axis) laser pulse propagating in a slab waveguide with dielectric walls at $|y|\geqslant R_{cap}$. The continuity of tangential x components of electric and magnetic fields of the laser at the boundary $y=R_{cap}$ requires the continuity of the transverse y derivative of the laser electric field (of its sole x component). To find this derivative at the boundary $y=R_{cap}+0$, we should use the linear equation (1) in the wall at $y\geqslant R_{cap}$, where $\varepsilon_0=\varepsilon_w>1$. In the comoving laser pulse variables $\xi=z-ct$, $\zeta=z$, $r_\perp=y$ [identical to Eq. (3) but dimensional] Eq. (1) has the form

$$\left\{ 2ik_0(1-\varepsilon_w)\frac{\partial}{\partial\xi}+\frac{\partial^2}{\partial r_\perp^2}+k_0^2(\varepsilon_w-1)\right\}\boldsymbol{E}_0=\mathbf{0}, \quad (28)$$

where the small derivatives along the ''propagation'' ζ variable, as well as the second derivative along ξ, were neglected as the length of the pulse $L\sim[\partial/(\partial\xi)]^{-1}$ is assumed to be much higher than the laser wavelength ($k_0L\gg1$), but much shorter than the laser pulse evolution length, which is determined by the diffraction, dispersion, and nonlinear interaction inside a capillary. The solution to this equation for a one component *S*-polarized laser field can be found in the form

$$\boldsymbol{E}_0=e_xE_{0x}, \quad E_{0x}=E(r_\perp,\xi)\exp(ik_{w\perp}r_\perp), \quad (29)$$

where E is the amplitude slowly varying on the scale $k_{w\perp}^{-1}$, for which Eq. (28) reads

$$\frac{\partial E}{\partial r_\perp}=\frac{k_0}{k_{w\perp}}(\varepsilon_w-1)\frac{\partial E}{\partial\xi}, \quad k_{w\perp}=k_0(\varepsilon_w-1)^{1/2}. \quad (30)$$

Equations (29) and (30) show that inside a dielectric wall

$$\frac{\partial E_{0x}}{\partial r_\perp}=ik_{w\perp}\left(1-\frac{i}{k_0}\frac{\partial}{\partial\xi}\right)E_{0x}. \quad (31)$$

As both the x component of the laser field and its y derivative are continuous at the boundary, Eq. (31) [with the perpendicular wave vector determined by Eq. (30)] gives the boundary condition for the laser wave equation (4) inside a slab dielectric capillary.

For a one-component *P*-polarized laser field, the boundary conditions in the slab geometry can be derived in the same way, taking into account the continuity of the magnetic field and of the electric field induction, which lead to the effective perpendicular wave vector (see, e.g., [37])

$$k_{w\perp}=k_0(\varepsilon_w-1)^{1/2}/\varepsilon_w. \quad (32)$$

So, for a rectangular wave guide (if the laser polarized along one of the waveguide walls), the laser pulse propagation inside the waveguide can be described by the scalar (one-component) Eq. (4) with the boundary conditions at the walls of the same type (31), but with different perpendicular wave vectors along the x and y axes.

In the case of a cylindrical waveguide the problem is more complicated as the scalar one-component field evidently cannot describe the field structure inside the capillary, as generally speaking, the field at the boundary is a composition of *S*- and *P*-polarized components, depending on the azimuthal angle. But for the field structure of the TE type [38] excited by a linear polarized laser pulse [21], the electric field of the laser had practically one component inside the capillary except for a thin layer at the waveguide wall. The accurate description of the field in this boundary layer is necessary for the correct definition of the laser pulse energy losses due to reflection and absorption in the wave-guide wall [39]. But a little bit apart from the wall inside the capillary, the laser field can be approximated by the sole component with the model boundary condition, which leads to the correct energy losses.

Further, we shall use this approximation to investigate laser pulse propagation in a cylindrical capillary solving the scalar one-component version of Eq. (4) [when the vector of the polarization in Eq. (2) is assumed to be linear] with the boundary condition (31) and with the effective perpendicular wave vector [40]

$$k_{w\perp}=k_0(\varepsilon_w-1)^{1/2}\frac{2}{\varepsilon_w+1}. \quad (33)$$

It is evident that expression (33) is the result of some ''averaging'' of boundary conditions for *S* and *P* polarizations, Eqs. (30) and (32). The direct solution of the linear stationary limit of scalar Eq. (4) (with the right-hand side equal to zero and $\partial/\partial\xi=0$) with the boundary conditions (31),(33) demonstrates exactly the same dissipation of eigenmodes [described by zero order Bessel functions $J_0(k_{\perp n}r)$], which is known from the solution to the dispersion equation of the problem with allowance made for the vector structure of the field [39,21],

$$\delta k_z''=\frac{u_n^2}{k_0R_{cap}^3}\frac{\mathrm{Re}(k_{w\perp})}{|k_{w\perp}|^2}=\frac{u_n^2}{2k_0^2R_{cap}^3}\frac{1+\varepsilon_w}{\sqrt{\varepsilon_w-1}}, \quad (34)$$

where u_n is the nth root of the equation $J_0(u_n)=0$ and $\delta k_z''$ is the imaginary part of the longitudinal (along the z axis) wave vector determining the exponential decrease of the laser field with the pulse propagation inside the capillary due to electromagnetic energy flux through the capillary walls.

III. GUIDED LASER PULSE PROPAGATION IN A WIDE CAPILLARY

To investigate a possibility of a guided propagation of intense laser pulses in wide gas-filled cylindrical capillaries, we solve numerically the set of equations (4), (12), and (27) with the boundary conditions at the capillary walls, Eqs. (31) and (33), and with the Gaussian laser pulse at the entrance of the capillary,

$$a(\xi,\rho,\zeta=0)=a_0\exp\left[-2\ln2\frac{(\xi-\xi_0)^2}{\omega_{p0}^2\tau_{imp}^2}-\frac{\rho^2}{k_{p0}^2r_0^2}\right], \quad (35)$$

where r_0 is the minimum radius of the laser pulse at the best vacuum focus, τ_{imp} is the full width at half maximum pulse duration, $a_0=eE_{0max}/(m\omega w_0c)$, and E_{0max} is the maximum laser electric field. The boundary conditions for the wake-field potential implies that $\Phi=1$ in the unperturbed plasma or gas in front of the pulse ($\xi\to\infty$) and at $r\to\infty$.

The radial profile of a gas density inside a capillary ($r\leqslant R_{cap}$) was assumed to be parabolic,

$$n_a(r)=n_{a0}\left[1+\frac{r^2}{R_{ch}^2}\right], \quad (36)$$

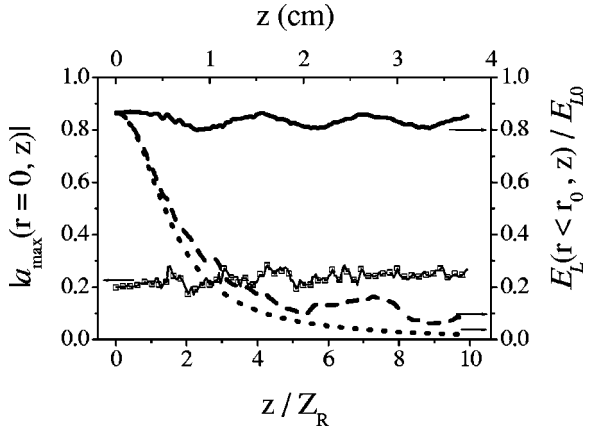

FIG. 1. The dependences of the normalized laser pulse energy in the initial spot size $E_L(r<r_0,z)/E_{L0}$ (lines) and the maximum of the laser pulse field on the axis $|a_{max}(r=0,z)|$ (square points) on the propagation distance z (normalized to the Rayleigh length $z_R=k_0r_0^2/2$, bottom axis, and measured in cm, top axis). The solid curve gives the laser pulse energy for the radial profile of a gas density (36), the dashed line for the capillary with a homogeneous gas profile $n_a(r\leqslant R_{cap})=n_{a0}=1.9\times10^{18}$ cm^{-3}, and the dotted line for the case of free diffraction in a vacuum. The parameters of the simulations are given in the text.

so that the density depression at the axis (in comparison with the gas density at the capillary walls) is determined by the ratio $(R_{cap}/R_{ch})^2$: $n(R_{cap})/n_{a0}=1+R_{cap}^2/R_{ch}^2$. As the density depression, which can be achieved practically by a spin of the capillary or by using piezoceramic tubes, is usually no more than 2, the radius of the channel in Eq. (36) for these cases should be no less than the radius of the capillary ($R_{cap}\leqslant R_{ch}$). In the results presented below the gas density at the capillary axis was chosen to be $n_{a0}=1.9\times10^{18}$ cm$^{-3}/Z_n$ and $R_{cap}=R_{ch}=125$ μm. In the region of complete gas ionization the electron density produced by OFI at the capillary axis is equal to $n_0(r=0)\equiv\mathcal{N}_0=1.9\times10^{18}$ cm^{-3}, and that for the laser wavelength $2\pi/k_0=0.8$ μm gives $\omega_0/\omega_{p0}=30$.

Figures 1 and 2 demonstrate the guided propagation of the laser pulse in a capillary (with glass walls, $\varepsilon_w=2.25$, and diameter 0.25 mm) filled with hydrogen. The laser pulse was focused onto the capillary entrance with the laser wavelength $2\pi/k_0=0.8$ μm, $r_0=31$ μm, $a_0=0.2$, $\tau_{imp}=100$ fs, $P_L=1.3$ TW, $q_L=0.86\times10^{17}$ W/cm^2. The initial laser spot size was matched with the channel radius by the linear condition [41,9]

$$r_0=(2R_{ch}/k_{p0})^{1/2}, \tag{37}$$

which, in the case of preionized unbounded plasma with the electron density profile (36), provides a guided propagation of a Gaussian laser pulse for $P_L/P_c\ll1$. The solid line in Fig. 1 shows the dependence of the normalized laser pulse energy in the initial spot size $E_L(r<r_0,z)/E_{L0}=\int_{-\infty}^{\infty}d\xi\int_0^{r_0}|a|^2dr(\int_{-\infty}^{\infty}d\xi\int_0^{R_{ch}}|a|^2dr)^{-1}$ on the propagation

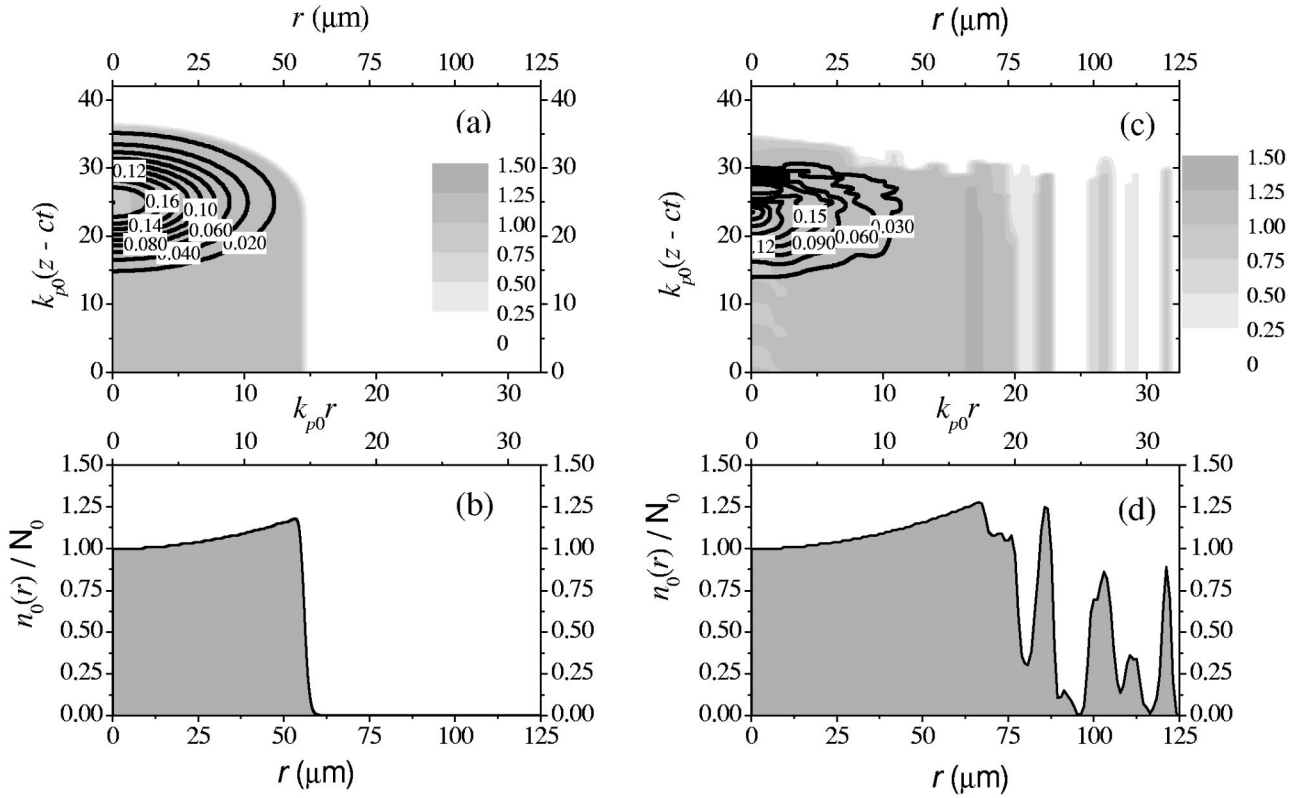

FIG. 2. Normalized electron plasma density $n(r,\xi)/\mathcal{N}_0$ (gray scale map) and the laser field $|a(r,\xi)|$ (contour lines) at the entrance of capillary $z=0$ (a) and at the propagation distance $z=3Z_R=1.13$ cm (c), and also the radial profiles of the plasma density produced by OFI $n_0(r,\xi\to-\infty)/\mathcal{N}_0$ at the same propagation distances $z=0$ (b) and $z=1.13$ cm (d). The parameters are the same as in Fig. 1.

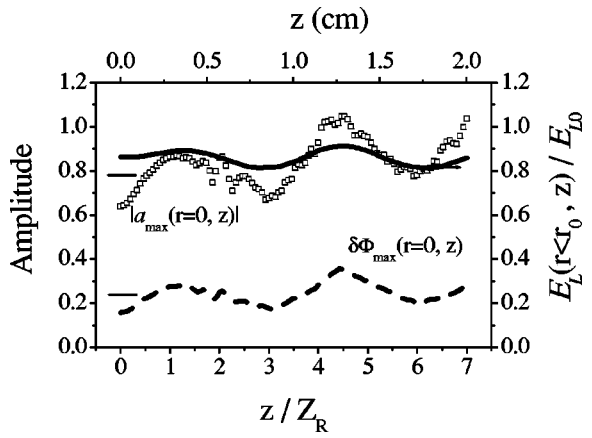

FIG. 3. Normalized laser pulse energy in the initial spot size $E_L(r<r_0,z)/E_{L0}$ (solid curve), the maximum of the laser pulse field on the axis $|a_{max}(r=0,z)|$ (square points), and the maximum of the wake-field potential on the axis behind the pulse $\delta\Phi_{max}=\Phi_{max}(r=0,z)-1$ (dashed line) as functions of propagation distance. The parameters of the simulation are given in the text.

distance z (normalized to the Rayleigh length $z_R=k_0r_0^2/2$). For comparison, the same dependences are shown for the capillary with a homogeneous gas profile $n_a(r\leqslant R_{cap})=n_{a0}=1.9\times10^{18}$ cm^{-3} (dashed line) and for the case of free diffraction in vacuum (dotted line). The scatter square points are the maxima of the laser pulse field on the axis. The periodic oscillations of the normalized laser pulse energy clearly seen in Fig. 1 (see also Figs. 3 and 7) are caused by the dependence of the matching condition (for the laser pulse propagation in a parabolic plasma channel without distortions) on the laser pulse power $P_L(\xi)$, which is different in different cross sections of the pulse. As was shown in [41], a small mismatch of condition (37), which is determined by $P_L(\xi)/P_c$, leads to harmonic oscillations of the laser pulse intensity in the plasma channel with the period πZ_R in conformity with the oscillations in Fig. 1.

Figure 2 illustrates the typical structures of the electron plasma density and also the laser field at the entrance of the capillary (a),(b) and at the propagation distance $z=3Z_R=1.13$ cm (c),(d). As the capillary diameter exceeds substantially the initial laser spot size, only the internal part of the gas at the capillary axis is ionized initially [Figs. 2(a) and 2(b)] producing the radial profile of the electron plasma density specific for a leaky channel. So, after propagation over a distance of the order of the Rayleigh length, a small part of the laser pulse diffracts up to the capillary walls. Due to reflection from the capillary walls a small intensity standing-wave pattern of the laser field produces by OFI a multilayer tubular structure of the electron density in the radial direction [Figs. 2(c) and 2(d)]. The obtained plasma density profile provides the guided propagation of the laser pulse over many Rayleigh lengths and effectively isolates waveguide walls from the high intensity part of the pulse, with the laser intensity contrast between the axis and the vicinity of the capillary wall of order 10^{-6}.

Figures 3 and 4 demonstrate the guided propagation of a more powerful laser pulse with $r_0=27$ μm, a_0

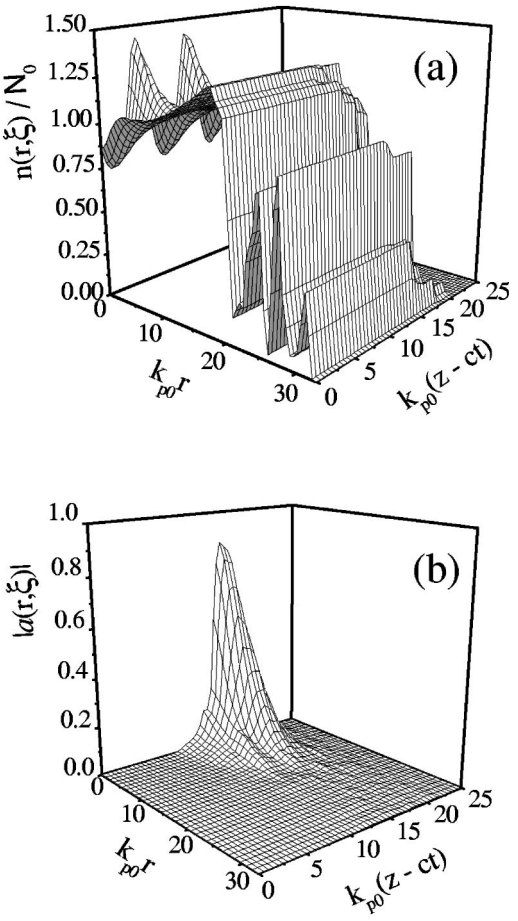

FIG. 4. Surface plots of the electron plasma density $n(r,\xi)/\mathcal{N}_0$ (a) and the normalized laser field $|a(r,\xi)|$ (b) at the propagation distance $z=4Z_R\approx1.2$ cm for the laser pulse with $r_0=27$ μm, $a_0=0.64$, $\tau_{imp}=45$ fs, $P_L=10$ TW, $q_L=0.88\times10^{18}$ W/cm^2 in, same as in Figs. 1–3 capillary ($\varepsilon_w=2.25$, $R_{cap}=125$ μm) filled with hydrogen.

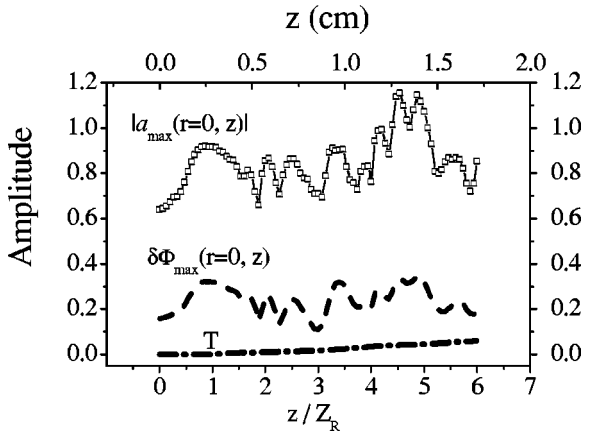

FIG. 5. Peak normalized laser pulse field on the axis $|a_{max}(r=0,z)|$ (square points), the maximum of the wake-field potential on the axis behind the pulse $\delta\Phi_{max}=\Phi_{max}(r=0,z)-1$ (dashed line), and the normalized transmission of the laser pulse energy through the capillary walls (dashed-dotted line) as functions of propagation distance. The parameters are the same as in Figs. 3 and 4, but the capillary is filled with helium.

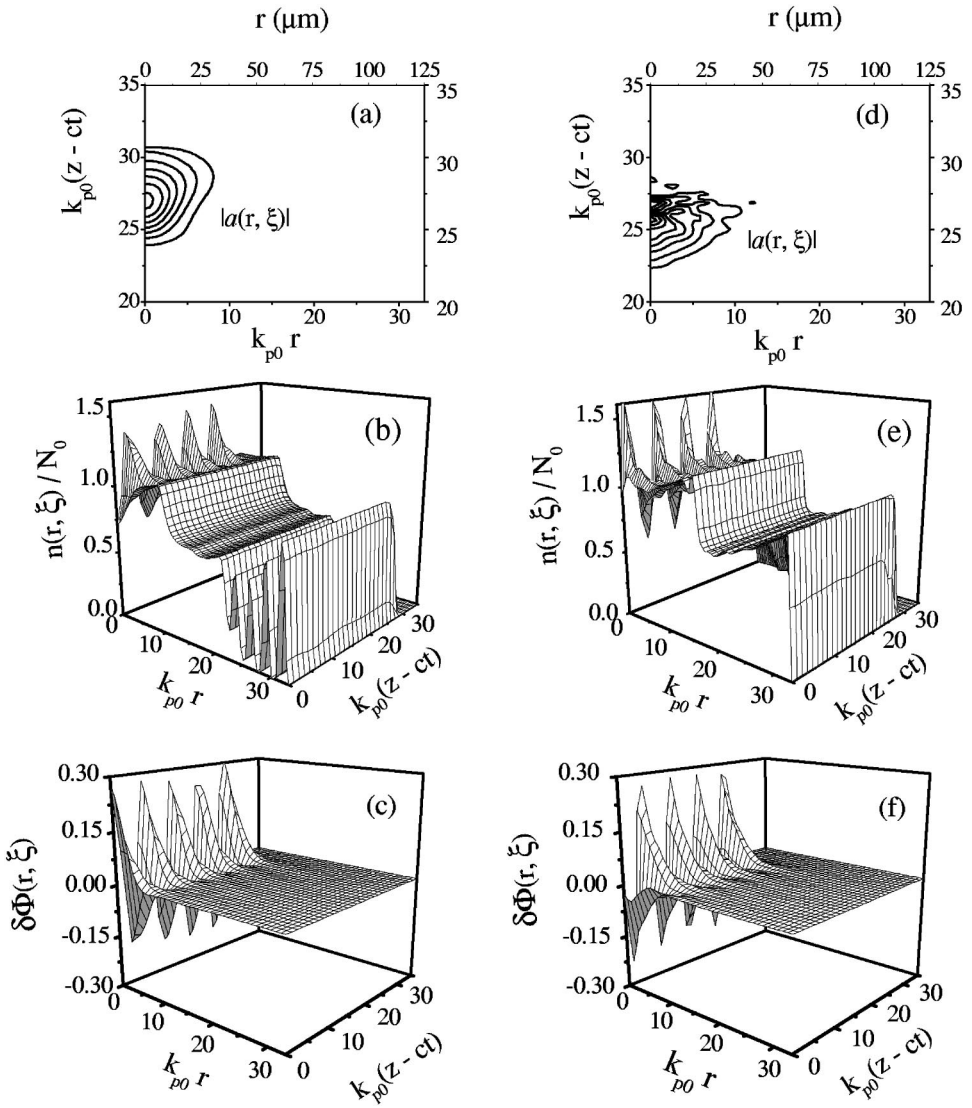

FIG. 6. Counter lines of the normalized laser field $|a(r,\xi)|$ (a),(d), surface plots of the electron plasma density $n(r,\xi)/\mathcal{N}_0$ (b),(e), and the wake-field potential $\delta\Phi=\Phi(r,\xi)-1$ (c),(f) at the propagation distances $z=Z_R \approx 0.29$ cm and $z=5Z_R \approx 1.43$ cm, respectively. The parameters are the same as in Fig. 5: laser pulse with $r_0=27$ μm, $\tau_{imp}=45$ fs, $P_L=10$ TW in the capillary ($\varepsilon_w=2.25$, $R_{cap}=125$ μm) filled with helium.

$=0.64$, $\tau_{imp}=45$ fs, $P_L=10$ TW, $q_L=0.88\times10^{18}$ W/cm^2 in the same capillary ($\varepsilon_w=2.25$, $R_{cap}=125$ μm) filled with hydrogen. As the laser pulse power was comparable with the critical one for relativistic self-focusing ($P_L/P_c \approx 0.7$) the laser pulse spot size was chosen slightly less than the matched radius (37). Figure 3 shows the dependences on the propagation distance z: the normalized laser pulse energy in the initial spot size (solid line), the maxima of the laser pulse field on the axis (scatter square points), and the maximum of the wake-field potential on the axis behind the pulse (dashed line). Figure 4 illustrates the typical structures of the electron plasma density [Fig. 4(a)] and also the laser field [Fig. 4(b)] at the propagation distance $z=4Z_R \approx 1.2$ cm. The comparison of Figs. 1 and 3 shows that self-focusing of the laser pulse with the maximum power slightly below the critical one leads to increased oscillations of the laser pulse with the period $\approx \pi Z_R$ in accord with [41], but at the same time, self-focusing increases the efficiency of the wake-field generation due to increased laser intensity at the capillary axis, and also improves the laser pulse channeling due to decreasing of the laser energy losses through the capillary walls. For the above parameters the laser pulse energy decay through the capillary walls is equal to 0.5% after propagation over a distance of 2 cm. If the same laser pulse with $r_0=27$ μm would propagate in a comparatively narrow capillary with $R_{cap} \approx r_0/0.65=42$ μm, which satisfies the condition of the best coupling into the main mode [18,21], the lowest energy losses (for the monomode propagation in a vacuum capillary) in accordance with Eq. (34) would be more than an order of magnitude higher ($\approx 7.5\%$ for the same propagation distance, 2 cm).

The propagation of the same laser pulse as in Figs. 3 and 4 in the same capillary ($\varepsilon_w=2.25$, $R_{cap}=125$ μm) but filled with helium is illustrated in Figs. 5 and 6. Due to substantial increase of the ionization potential (for a total ionization of helium), the fully ionized plasma channel is smaller in diameter than the channel diameter in the capillary filled with hydrogen [compare Figs. 4(a) and 6(b) and 6(e)]. This leads to increased leakage of the laser energy from the channel that involves an increase of reflection from the capillary walls and the laser pulse decay due to transmission through the walls. The increased reflection from the capillary walls manifests itself in the pronounced oscillations and distortions of the laser pulse as it propagates along the capillary

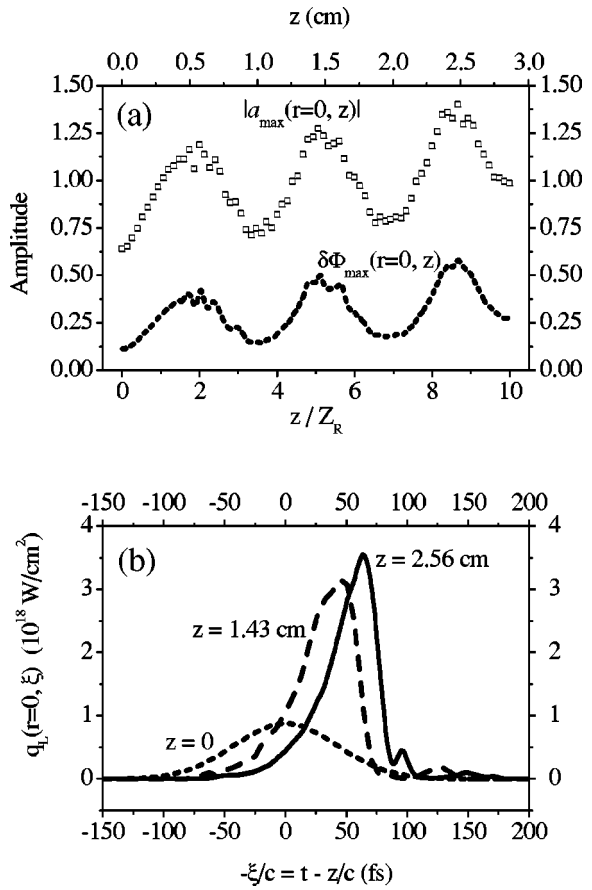

FIG. 7. Peak normalized laser pulse field on the axis $|a_{max}(r=0,z)|$ (square points) and the maximum of the wake-field potential on the axis behind the pulse $\delta\Phi_{max}=\Phi_{max}(r=0,z)-1$ (dashed line) as functions of propagation distance, (a) and (b): pulse intensity on the axis $q_L(r=0,\xi)$ at $z=0$ (dotted line), $z=1.43$ cm (dashed line), and $z=2.56$ cm (solid line). Parameters are the same as in Figs. 3 and 4 except for the longer laser pulse duration $\tau_{imp}=100$ fs instead of 45 fs.

[see Figs. 5 and 6(d)]. Nevertheless the pulse is guided over many Rayleigh lengths and generates effectively a regular wake field suitable for electron acceleration, as follows from Figs. 6(c) and 6(f). It should be noted also that even enhanced transmission of the laser pulse energy through the capillary walls (dashed-dotted line in Fig. 5) still does not exceed the minimal energy losses (34) for the monomode propagation in a vacuum capillary with $R_{cap}\approx r_0/0.65=42$ μm.

A simulation similar to Figs. 3 and 4 with $\tau_{imp}=100$ fs instead of 45 fs exhibits increased oscillations of the laser pulse intensity and wake-field potential [Fig. 7(a)] but at the same time demonstrates more efficient generation of the wake field due to the processes of laser pulse self-focusing and shortening. Figure 7(b) shows that at $z=2.56$ cm the peak intensity has increased by a factor of 4 and the pulse duration is two times less in comparison with the initial values at $z=0$. The growth of the laser pulse amplitude in the back of the pulse with the sharp drop after the peak is attained, and also the intensity modulation of the rear part of the pulse with the scale of order $2\pi/\omega_{p0}$ point to the processes of self-phase modulation, group velocity dispersion, and self-modulation instability [10,42,43]. Note that the initial pulse length $\tau_{imp}=100$ fs was more than three times longer than the optimal length, 30 fs, for the resonant excitation of a wake field and was slightly longer than the plasma wave period ($\omega_{p0}\tau_{imp}=7.85$).

IV. CONCLUSIONS

We investigate short intense laser pulse channeling in gas-filled capillaries. The guided laser pulse propagation and wake-field generation were studied in a wide (in comparison with the laser spot size) capillary, with a relatively small gas density depletion on the capillary axis, which can be produced by a high-speed rotation of the capillary around its axis or by radially propagating shock waves generated in a piezoceramic tube. The set of basic equations was formulated with allowance made for the finite pulse length effects, plasma formation due to tunneling ionization of a gas, atomic electron, and relativistic effects, and laser energy losses due to optical field ionization and transmission through the capillary walls. Special attention was paid to the proper nonstationary boundary conditions for the one-component linear polarized laser field at the cylindrical capillary wall. The results include (i) a derivation of a single equation for the wake-field potential, which describes the fully relativistic plasma response in the presence of optical field ionization of a gas, (ii) a demonstration of guided propagation of a short intense laser pulse over many Rayleigh lengths in a leaky plasma channel produced by the pulse due to OFI in a radially inhomogeneous gas filling a capillary, and (iii) laser pulse compressing and focusing during channel-guided propagation in a gas-filled capillary, and (iv) an efficient generation of a regular wake field over long distances suitable for laser wake-field accelerators.

ACKNOWLEDGMENTS

This work was supported by the Satellite Venture Business Laboratory of the Utsunomiya University, Japan by the Russian Foundation for Basic Research, Grant No. 01-02-16723, and by the INTAS Project No. 97-10236.

[1] E. Esarey *et al.*, IEEE Trans. Plasma Sci. **24**, 252 (1996), and references therein.

[2] IEEE Trans. Plasma Sci. **21**, 1 (1993), IEEE special issue on generation of coherent radiation using plasmas, edited by W. B. Mori.

[3] H. M. Milchberg, C. G. Durfee III, and T. J. McIlrath, Phys. Rev. Lett. **75**, 2494 (1995).

[4] P. B. Corkum *et al.*, Phys. Rev. Lett. **62**, 1259 (1989).

[5] A. Y. Goltsov, D. V. Korobkin, YI. Ping, and S. Suckewer, J. Opt. Soc. Am. B **17**, 868 (2000).

[6] A. B. Borisov *et al.*, Phys. Rev. A **45**, 5830 (1992).
[7] B. Hafizi, A. Ting, P. Sprangle, and R. F. Hubbard, Phys. Rev. E **62**, 4120 (2000), and references therein.
[8] P. Sprangle and E. Esarey, Phys. Fluids B **4**, 2241 (1992); R. F. Hubbard *et al.*, Phys. Rev. E **63**, 036502 (2001).
[9] N. E. Andreev, L. M. Gorbunov, V. I. Kirsanov, K. Nakajima, and A. Ogata, Phys. Plasmas **4**, 1145 (1997); N. E. Andreev, L. M. Gorbunov, and A. A. Frolov, Fiz. Plazmy **24**, 888 (1998) [Plasma Phys. Rep. **24**, 825 (1998)].
[10] E. Esarey, C. B. Schroeder, B. A. Shadwick, J. S. Wurtele, and W. P. Leemans, Phys. Rev. Lett. **84**, 3081 (2000).
[11] C. G. Durfee III and H. M. Milchberg, Phys. Rev. Lett. **71**, 2409 (1993); T. R. Clark and H. M. Milchberg, Phys. Rev. E **61**, 1954 (2000).
[12] P. Volbeyn, E. Esarey, and W. P. Leemans, Phys. Plasmas **6**, 2269 (1999).
[13] E. W. Gaul, S. P. Le Blanc, A. R. Rundquist, R. Zgadzaj, H. Langhoff, and M. C. Downer, Appl. Phys. Lett. **77**, 4112 (2000).
[14] A. Zigler, Y. Ehrlich, C. Cohen, J. Krall, and P. Sprangle, J. Opt. Soc. Am. B **13**, 68 (1996); D. Kaganovich *et al.*, Phys. Rev. E **59**, R4769 (1999); P. Sprangle *et al.*, *ibid.* **63**, 056405 (2001).
[15] S. M. Hooker, D. J. Spence, and R. A. Smith, J. Opt. Soc. Am. B **17**, 90 (2000).
[16] T. Hosokai *et al.*, Opt. Lett. **25**, 10 (2000).
[17] D. J. Spence and S. M. Hooker, Phys. Rev. E **63**, 015401 (2000); D. J. Spence, A. Butler, and S. M. Hooker, J. Phys. B **34**, 4103 (2001).
[18] B. Cros, C. Courtois, G. Malka, G. Matthieussent, J. R. Marqus, F. Dorchies, F. Amiranoff, S. Rebibo, G. Hamoniaux, N. Blanchot, and J. L. Miquel, IEEE Trans. Plasma Sci. **28**, 1071 (2000); C. Courtois, A. Couairon, B. Cros, J. R. Marqus, and G. Matthieussent, Phys. Plasmas **8**, 3445 (2001).
[19] S. Jackel *et al.*, Opt. Lett. **20**, 1086 (1995).
[20] M. Borghesi *et al.*, Phys. Rev. E **57**, 4899 (1998).
[21] F. Dorchies *et al.*, Phys. Rev. Lett. **82**, 4655 (1999).
[22] K. Nakajima (private communication).
[23] M. V. Ammosov, N. B. Delone, and V. P. Krainov, Zh. Éksp. Teor. Fiz. **91**, 2008 (1986) [Sov. Phys. JETP **64**, 1191 (1986)]; N. B. Delone and V. P. Krainov, Usp. Fiz. Nauk **168**, 531 (1998) [Phys. Usp. **41**, 469 (1998)].
[24] P. Sprangle, E. Esarey, and B. Hafizi, Phys. Rev. E **56**, 5894 (1997); P. Sprangle, B. Hafizi, and P. Serafim, *ibid.* **59**, 3614 (1999).
[25] N. E. Andreev, M. E. Veisman, M. G. Cadjan, and M. V. Chegotov, Fiz. Plazmy **26**, 1010 (2000) [Plasma Phys. Rep. **26**, 947 (2000)]; M. V. Chegotov, *ibid.* **26**, 940 (2000) [*ibid.* **26**, 881 (2000)].
[26] N. E. Andreev, M. V. Chegotov, and M. E. Veisman, IEEE Trans. Plasma Sci. **28**, 1098 (2000).
[27] V. P. Kandidov, O. G. Kosareva, and S. A. Shlenov, Quantum Electron. **24**, 971 (1994).
[28] M. V. Chegotov, Proc. SPIE **3683**, 33 (1999).
[29] N. E. Andreev, M. V. Chegotov, M. E. Veisman, B. He, and J. T. Jhang, Proc. SPIE **3735**, 234 (1999); N. E. Andreev, M. E. Veisman, S. P. Goreslavskii, and M. V. Chegotov, Fiz. Plazmy **27**, 296 (2001) [Plasma Phys. Rep. **27**, 278 (2001)].
[30] V. B. Gil'denburg, V. I. Pozdnyakova, and I. A. Shereshevskii, Phys. Lett. A **203**, 214 (1995).
[31] P. Mora and T. M. Antonsen, Jr., Phys. Plasmas **4**, 217 (1997).
[32] N. E. Andreev, M. V. Chegotov, M. E. Veisman, T. Auguste, P. D'Oliveira, S. Hulin, P. Monot, A. Ya. Faenov, T. A. Pikuz, A. I. Magunov, I. Yu. Skobelev, F. B. Rosmej, and M. Yu. Romanovskii, JETP Lett. **68**, 592 (1998).
[33] N. E. Andreev, M. V. Chegotov, M. C. Downer, E. W. Gaul, N. H. Matlis, A. A. Pogosova, and A. R. Rundquist, IEEE Trans. Plasma Sci. **28**, 1090 (2000).
[34] P. Sprangle, E. Esarey, and A. Ting, Phys. Rev. Lett. **64**, 2011 (1990).
[35] N. E. Andreev, E. V. Chizhonkov, A. A. Frolov, and L. M. Gorbunov, Nucl. Instrum. Methods Phys. Res. A **410**, 469 (1998).
[36] P. Sprangle, E. Esarey, J. Krall, and G. Joyce, Phys. Rev. Lett. **69**, 2200 (1992); J. Krall, E. Esarey, P. Sprangle, and G. Joyce, Phys. Plasmas **1**, 1738 (1994).
[37] N. E. Andreev, C. Courtois, B. Cros, L. M. Gorbunov, and G. Matthieussent, Phys. Rev. E **64**, 016404 (2001).
[38] E. A. J. Marcatili and R. A. Schmeltzer, *Hollow Metallic and Dielectric Waveguides for Long Distance Optical Transmission and Lasers*, Bell Syst. Tech. J. **43**, 1783 (1964).
[39] B. Cros, C. Courtois, G. Matthieussent, A. Di Bernardo, D. Batani, N. Andreev, and S. Kuznetsov, Phys. Rev. E **65**, 026405 (2002).
[40] A. Solodov (private communication).
[41] N. E. Andreev, V. I. Kirsanov, and L. M. Gorbunov, Phys. Plasmas **2**, 2573 (1995).
[42] R. F. Hubbard, P. Sprangle, and B. Hafizi, IEEE Trans. Plasma Sci. **28**, 1122 (2000).
[43] C. Ren, B. J. Duda, R. G. Hemker, W. B. Mori, T. Katsouleas, T. M. Antonsen, Jr., and P. Mora, Phys. Rev. E **63**, 026411 (2001).